Femtosecond filamentation in turbulent air

A. Houard,[1] M. Franco,[1] B. Prade,[1] A. Durécu,[2] L. Lombard,[2] P. Bourdon,[2] O. Vasseur,[2] B. Fleury,[3] C. Robert,[3] V. Michau,[3] A. Couairon,[4,*] and A. Mysyrowicz[1]

[1]*Laboratoire d'Optique Appliquée, ENSTA-Ecole Polytechnique, CNRS, F-91761 Palaiseau, France*

[2]*Département d'Optique Théorique et Appliquée, ONERA, 91761 Palaiseau, France*

[3]*Département d'Optique Théorique et Appliquée, ONERA, 92322 Chatillon, France*

[4]*Centre de Physique Théorique, École Polytechnique, CNRS, F-91128 Palaiseau, France*

(Received 6 June 2008; published 5 September 2008)

The influence of air turbulence on femtosecond laser filamentation is studied experimentally and numerically for laser powers of a few critical powers. Air turbulence in the path of the beam prior to filamentation induces a large pointing and formation instability attributed to an increase of the self-focusing distance and higher modulational instability in the presence of turbulence. By contrast, previously formed filaments are robust both in terms of beam pointing accuracy and survival when crossing turbulent air.

DOI: 10.1103/PhysRevA.78.033804 PACS number(s): 42.65.Jx, 42.68.Bz, 42.25.Dd, 42.65.Sf

I. INTRODUCTION

An increasing interest is devoted to the study of femtosecond filamentation. From a fundamental point of view, it provides an interesting system where very strong optical nonlinearities compete to yield remarkably stable structures called filaments, which generate long plasma channels and are able to transmit very high intensities over large distances [1,2]. In turn, this effect has been exploited in many applications such as remote sensing of distant targets, broadband light detection and ranging (LIDAR) detection of pollutants [3], guiding and triggering of electric discharges [4], or generation of THz radiation [5,6]. Many foreseen applications rely on the presence of filaments at very long distances, exceeding hundreds of meters. Therefore an important concern is the influence of air turbulence on the filamentation process and on the filament characteristics.

Air turbulence is usually characterized by a structure constant C_n^2 which determines the intensity of fluctuations of the refractive index [7,8]. Values of C_n^2 between 10^{-15} and 10^{-13} $m^{-2/3}$ represent standard atmospheric turbulence. Air turbulence can influence both the pointing accuracy (transverse filament wandering) and the distance at which filaments are formed (longitudinal filament wandering). The problem of filament wandering along the propagation axis z was investigated by Penano *et al.* who came to the conclusion that air turbulence should lead to an increase of the distance required for filament formation with chirped pulses when the structure constant C_n^2 is increased [9]. In contrast, Kandidov *et al.* showed from numerical simulations with a given $C_n^2=1\times10^{-11}$ $m^{-2/3}$ that the distance at which the intensity in the nonlinear focus reaches the ionization threshold is random for the different realizations (shots) but that on the average, turbulence should lead to a shorter collapse distance [10]. The major difference between the two studies is that Kandidov *et al.* considers pulse power many times exceeding critical power for self-focusing, resulting in multifilamentation of the laser beam. These results highlight the fact that in the presence of turbulence, filaments resulting from self-focusing and collapse of the whole beam exhibit different features from those resulting from modulational instability of the beam inhomogeneity [11]. Self-focusing of the whole beam should prevail for sufficiently weak air turbulence and input powers so as to form only one filament. An understanding of the competition between beam self-focusing and modulational instability in turbulent air is required to achieve control of longitudinal features of filaments, as, e.g., the filamentation length [12] or the filament concatenation [13,14].

Radial pointing stability was studied experimentally and numerically [15]. Measurements of the filament position after 30 and 100 m exhibit random isotropic displacements in good agreement with simulation results. Strong but localized turbulence placed in the zone after the onset of filamentation was found to barely affect the radial stability [16] while extended turbulence does not reduce significantly the survival rate of filaments [17]. It has been argued that the pointing accuracy of already formed filaments should be rather insensitive to turbulence because of the transverse dimension of a filament, smaller by a factor of 10 than the inner scale $l_0=1$ mm characterizing air turbulence. This scenario relies on the concept that the filament behaves as a narrow beam which does not depend on the periphery of the intense core. However, it was established that in the absence of air turbulence, a filament is sustained by an energy flux from the low intensity energy reservoir to the intense core [18]; energy losses via multiphoton absorption would rapidly dissipate the energy of the narrow filament if it was not refilled by this energy flux [19]. Specific experiments have established the validity of this scenario [20,21] and numerical simulations allowed a careful monitoring of the conical energy flux established during filamentation [22,23]. Since the transverse dimension of the energy reservoir surrounding a filament in air is larger than the inner scale of the Kolmogorov spectrum, the low intensity part of the beam must be sensitive to air turbulence; the energy flux and the survival probability of a filament should be correlated to this sensitivity.

No quantitative measurement has been done so far to interpret the interplay between filaments in turbulent air and their energy reservoir. In this work we use well-calibrated turbulence cells to investigate filamentation in air as a func-

*Corresponding author. couairon@cpht.polytechnique.fr

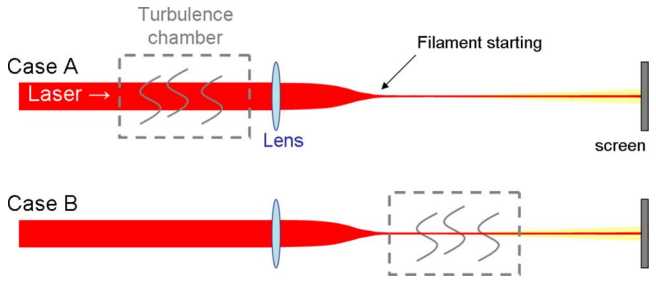

FIG. 1. (Color online) Experimental setup. Case A: turbulence is applied on the beam prior to filamentation and a camera records for each shot the white light spot on a screen placed 7 m after the focusing lens. The distance between the aperture and the entrance of the turbulence cell is 10 cm and the distance between the output plane of the cell and the lens is 30 cm. Case B: turbulence is applied on the filament after the self-focusing of the beam. The distance between the aperture and the lens is 270 cm.

tion of the intensity of turbulence. We study the effect of turbulence on the transverse wandering. We also explore whether turbulence decreases or increases the distance of collapse. We study two cases separately: Turbulence in the path of the beam prior to collapse (case A) and after filamentation (case B). The study is restricted to the case where only a single filament is formed. Numerical simulations are performed for both cases A and B and the effect of transverse wandering is statistically analyzed.

II. EXPERIMENTAL PROCEDURE

The experimental setup is shown in Fig. 1. The laser used is a CPA (chirped-pulse amplifier) Ti:sapphire laser chain delivering 50 fs pulses at 800 nm, with an energy per pulse of 15 mJ maximum at a repetition rate of 100 Hz. The beam has an apertured Gaussian beam resulting in a super-Gaussian profile with a diameter $w_0=1.5$ cm (half width at half maximum). In order to have a single filament, we restricted the initial laser peak power to a few P_{cr}, where P_{cr} ~ 3 GW is the minimum power necessary to form a filament in nonturbulent air at atmospheric pressure, using a 50 fs long laser pulse at 800 nm. It was predicted that atmospheric turbulence increases the power threshold for beam collapse P_c [7,24] by the condition

$$\frac{P_c}{P_{cr}} = 1 + \frac{3}{4}k_0^2 a^2 \left(\frac{aC}{2}\right)^{2/3}, \tag{1}$$

$$C = 4.38 l_0^{-1/3} C_n^2 \left\{1 - \left[1 + 17.5\frac{a^2}{l_0^2}\right]^{-1/6}\right\}, \tag{2}$$

where k_0 denotes the wave number of the laser pulse, $a = w_0/\sqrt{2}$ the width of an initial Gaussian beam $\mathcal{E} = \mathcal{E}_0 \exp(-r^2/2a^2)$, and $l_0=1$ mm, the inner scale of turbulence. For $C_n^2=10^{-13}$ m$^{-2/3}$, the condition (2) gives P_c $\sim 6.4P_{cr}$. Pulses with 3 mJ energy after a circular aperture were used, having therefore peak power of about $18P_{cr}$. This is about three times the required value for collapse in turbulent air with the smallest C_n^2. In order to reduce the distance required for collapse and filamentation, the beam was focused with a 4 m focal lens. Under these conditions, all our experiments led to the observation of a single filament.

The long calibrated turbulence chamber has been described elsewhere [25]. It consists of a 2.3 m long box in which hot air (up to 60 °C) is blown in and out laterally to achieve uniform turbulent flow. The C_n^2 factor defining the turbulence is calibrated inside the chamber with a CT meter, which is a microthermic probe measuring the local temperature structure constant C_T. The C_n^2 is then determined using the relation

$$C_n = \frac{79 \times 10^{-6} P}{T^2} C_T,$$

where P and T are, respectively, the gas pressure (in millibar) and temperature (in Kelvin) in the turbulent chamber [26]. The C_n^2 could be varied between $C_n^2=10^{-13}$ and 10^{-10} m$^{-2/3}$. This corresponds to propagation distances in air of 1 km under typical conditions ranging from very quiet to regular weather. Experiments have been performed by putting the turbulent air region before (case A) or after the onset of filamentation (case B) as shown in the figure.

During the filamentation process the laser pulse experiences a large self-phase modulation, generating a white light emission in the forward direction [1]. This white light continuum is used as a criterion to determine the presence of a filament and to measure its location in the plane perpendicular to the propagation axis. A synchronized charge coupled device (CCD) camera with a BG39 SCHOTT glass filter removing the fundamental component of the pulse around 800 nm took pictures of this white light emission spot on a diffusing screen with a flat spectral reflectivity placed 7 m after the focusing lens (see Fig. 1). The camera is an ANDOR DU434 CCD with an array of 1024×1024 pixels of 13 μm, yielding a resolution of 100 μm on the screen. For each measurement 256 pictures were recorded at 10 Hz. The pointing stability was evaluated by calculating the standard deviation σ of the position of the intensity maximum. Knowing that in the absence of turbulence filament formation occurs for every shot, the counting rate of white light emission corresponds to the probability of filament formation for a beam crossing a turbulence in case A whereas it gives the filament survival rate when it crosses a turbulent region in case B. In each case the position of the white spots is compared to the center of gravity of a low intensity beam (average diameter in the turbulence chamber ~ 1 mm) for which a filament is never formed.

Due to mechanical vibrations in the amplifier of the laser chain, the ir laser beam pointing presents a small instability in the horizontal plane. This is seen, for instance, in Fig. 2(a) showing the superposition of 200 shots of the low intensity beam center in the absence of turbulence. To correct this spatial anisotropy the horizontal spread of the points is reshaped to present the same standard deviation as the vertical one. This treatment is justified by the tacit assumption that the effects of turbulence are isotropic. The resulting distribution is plotted in Fig. 2(b).

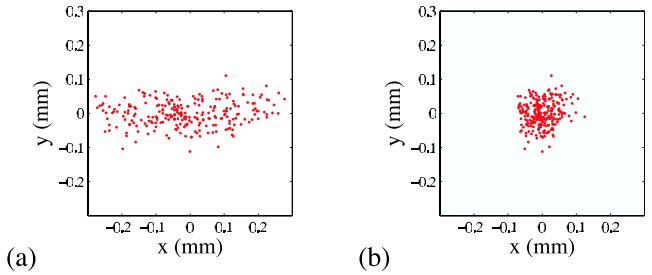

FIG. 2. (Color online) Position of the 100 μJ beam center in the absence of turbulence before (a) and after (b) horizontal reshaping.

III. EXPERIMENTAL RESULTS

A typical result for the beam wandering is shown in Fig. 3. Figure 3(a) shows the positions of the filaments in case A (turbulence before the onset of filamentation); Fig. 3(b) the position of the filaments in case B (turbulence after the onset of filamentation). We performed a systematic statistical analysis of the transverse displacements as a function of turbulence. Figures 4 and 5 show examples for the fluence distribution of white light recorded on the screen (a) and the distribution of the transverse position of the filaments (b) in case A, for $C_n^2=1.7\times10^{-11}$ m$^{-2/3}$ and $C_n^2=2.1\times10^{-13}$ m$^{-2/3}$, respectively. It is well-established that under the assumption of uniform and isotropic turbulence, the vertical and horizontal positions of the hot spots should independently follow a normal distribution law with the same variance, since air turbulence is a stochastic process. This means that the distance from the propagation axis (center of the beam at $r=0$) must be correctly described by a Rayleigh distribution law:

$$\Psi_R(r) = 1 - \exp(-r^2/w_R^2), \tag{3}$$

where w_R characterizes the width of the distribution. This result was established by Chin *et al.* [15] in the case of filaments analyzed after propagation distances of 30 and 105 m in turbulent air. Our experiments partly agree with this result, but also show different distributions interpreted as due to a stronger influence of nonlinear effects than that of turbulence on the transverse wandering. Figures 4(c) and 5(c) show the histogram of the hot spot (i.e., maximum intensity) distances from the axis for strong and very weak

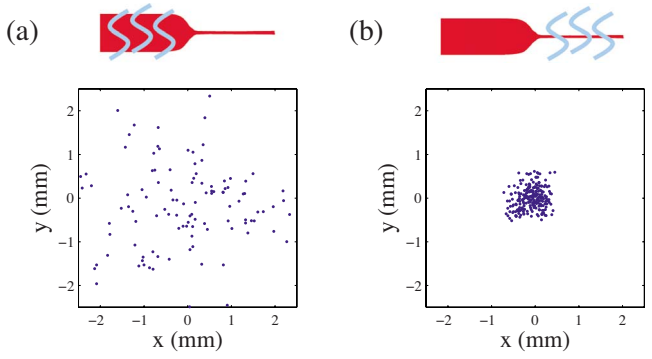

FIG. 3. (Color online) Position of the filament white light spot on the screen in cases A (a) and B (b) for a turbulence parameter of $C_n^2=1.7\times10^{-11}$ m$^{-2/3}$.

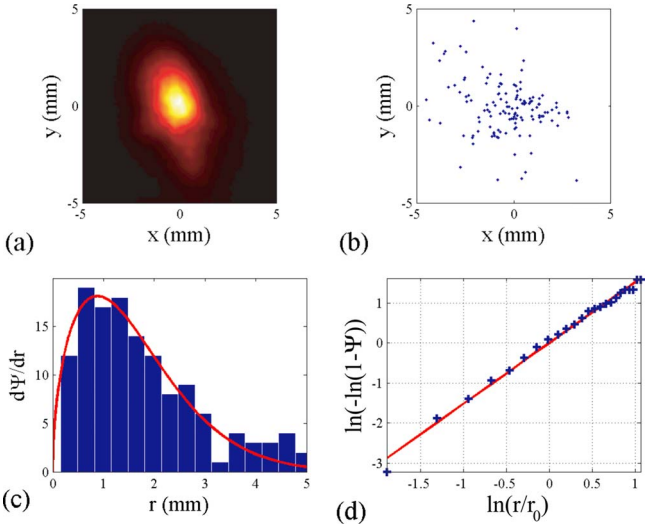

FIG. 4. (Color online) Experimental results for 256 shots in case A with strong turbulence $C_n^2=1.7\times10^{-11}$ m$^{-2/3}$. (a) Example of beam cross section at 7 m beyond the entrance of the turbulence cell. (b) Filament positions after correction of the systematic error in the horizontal direction. 127 (49%) shots were retained for which filamentation occurred. (c) Histogram of the transverse displacements fitted by a Weibull probability distribution [continuous curve in (c) and (d)] with parameters $p=1.52$ and $w_W=1.78$ mm. (d) details the fit procedure which amounts to determining the slope of the function $\ln[-\ln(1-\Psi)]$ of the cumulated number Ψ of filaments found within a circle of radius r.

turbulence. These histograms cannot be fitted perfectly with Rayleigh distribution law. In this case, the best fit of the distribution of filaments was obtained by using a Weibull distribution law:

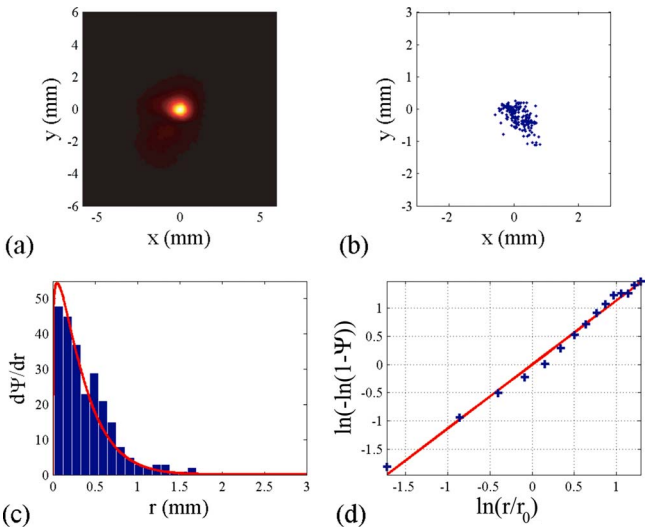

FIG. 5. (Color online) Experimental results presented as in Fig. 4 for 251 shots (98%) in case A with very weak turbulence $C_n^2=2.1\times10^{-13}$ m$^{-2/3}$. The Weibull distribution of transverse displacements [continuous curve in (c) and (d)] has parameters $p=1.13$ and $w_W=0.41$ mm.

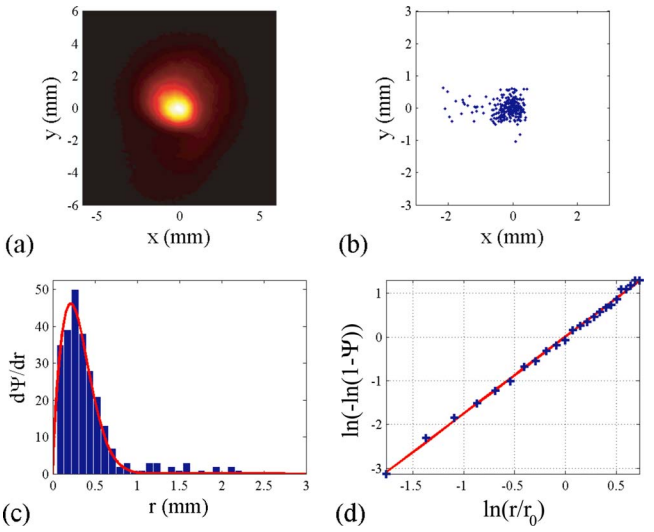

FIG. 6. (Color online) Experimental results presented as in Fig. 4 for 233 shots (91%) in case B with strong turbulence $C_n^2 = 1.7 \times 10^{-11}$ m$^{-2/3}$. The Weibull distribution of transverse displacements [continuous curve in (c) and (d)] has parameters $p = 1.76$ and $w_W = 0.35$ mm.

$$\Psi_W(r) = 1 - \exp(-r^p/w_W^p), \tag{4}$$

which generalizes the Rayleigh distribution law (both coincide for $p=2$). In our statistical analysis, we will fit the distribution of filaments by plotting the quantity $\ln[-\ln(1-\Psi)]$, depending on the cumulated number Ψ of hot spots located within a circle of diameter r, as a function of r for each interval of the histograms [see Figs. 4(d) and 5(d)]. This allows for a determination of the parameters w_W and p for the Weibull distribution, the magnitude of $|p-2|$ indicating the departure from a Rayleigh distribution. The corresponding density of probability $P = d\Psi/dr$ is then compared to the experimental histogram [continuous curve in (c)].

Figures 4 and 5 show that the distribution of the transverse position of the filaments in case A can be well-described by a Weibull probability distribution. This distribution is close to a Rayleigh distribution function only in the case of the strongest intensities of turbulence ($C_n^2 \geqslant 10^{-11}$ m$^{-2/3}$). A decrease of the turbulence intensity leads to a decrease in the averaged amplitude of the transverse wandering of filaments.

Figure 6 shows a similar statistical analysis performed in case B. One can notice that the transverse displacements are much smaller in this case, where the filament is already formed where the beam crosses the turbulent region.

Figure 7 gives results for the pointing stability in cases A and B as a function of the turbulence in the chamber. Also shown is the pointing stability of a similar beam with much lower intensity (black diamonds) propagating linearly in the whole path. According to Ref. [27] for linear propagation the mean square of the transverse displacement δr of the beam on the screen can be expressed as

$$\langle (\delta r)^2 \rangle = 2.91 \int_0^L C_n^2(z) w(z)^{-1/3} dz, \tag{5}$$

where w is the beam width and L is the propagation length in the turbulent medium. This law is shown as a dashed curve

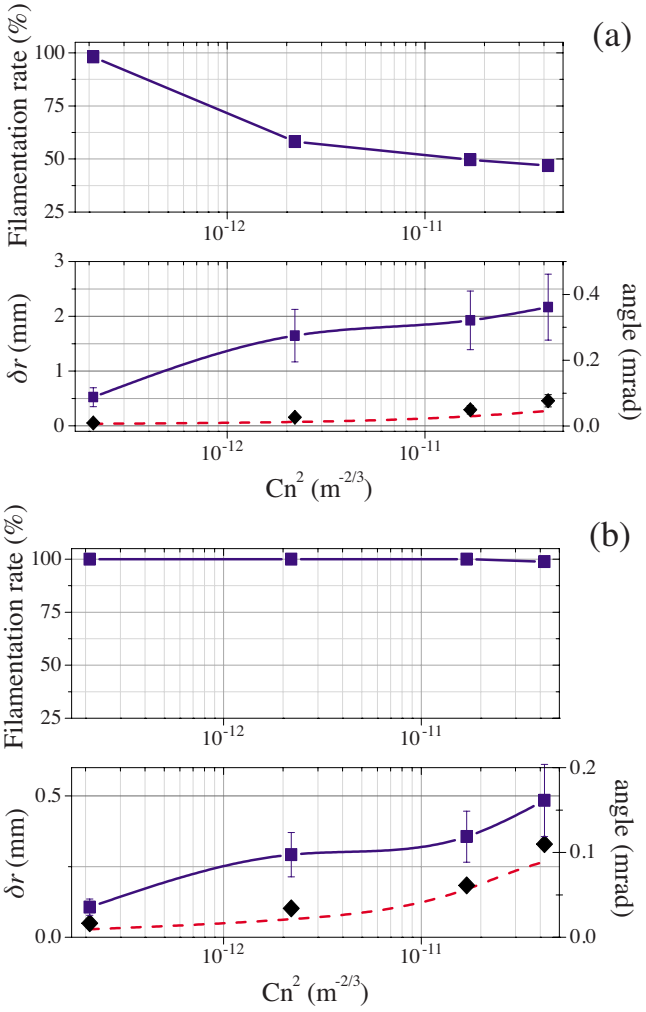

FIG. 7. (Color online) Filamentation rate (top) and average filament deviation $\langle \delta r \rangle$ (bottom) of a 3 mJ laser beam as function of the C_n^2 (in m$^{-2/3}$) in the chamber for case A (a) and B (b). The black diamonds show the deviation for a 100 μJ pulse propagating linearly under the same turbulent conditions, and the dashed red curve is a calculation using formula (5).

in Fig. 7 and fits rather well our measurements with the low intensity beam which were performed as benchmarks for the measurements of the transverse wandering of filaments. In the fully nonlinear regime, one can see that turbulence on the path of the beam prior to the onset of filamentation (case A) has a drastic effect on both the filament survival probability and pointing stability. By contrast the filament survival probability is largely insensitive to turbulence if it is formed before reaching the turbulent cell (case B), but the pointing instability is still larger than for linear beam propagation in the same conditions.

These results are in keeping with the model of the energy reservoir: In case A, the whole beam undergoes the effect of air turbulence before it is focused to form a filament. The energy reservoir is therefore not organized so as to sustain a perfectly cylindrically symmetric energy flow toward the propagation axis, but the filament can still form when turbulence is not strong enough to prevent the energy flux from accumulating power above P_{cr} around an intensity peak of

the beam. This results in a striking effect of turbulence on the filament formation probability rate in case A. Indeed, with the increase of the C_n^2 parameter the probability to form a filament decrease from 97% to 50%. This is in agreement with the conclusions of Penano *et al.* that turbulence increases the distance required for the onset of filamentation in the case of filaments resulting from self-focusing of the whole beam. This result is not expected to be always true; as discussed below, larger beam powers and a regime of modulational instability enhanced by turbulence may lead to the opposite conclusion.

In contrast, in case B, the energy flux is organized in nonturbulent air and is perfectly symmetric at the entrance of the turbulence cell. The strong nonlinear effects occurring in the filament core, in particular multiphoton absorption, act as a driving force which prevails over the effects of turbulence to keep the center of symmetry of the energy flux located on, or close to, the propagation axis. The energy reservoir refilling the central filament is about 1 mm large (corresponding Rayleigh length ~4 m) and is therefore not affected by turbulence, except for a tilt. Therefore once formed the filament is very robust against destruction by turbulence. However, the reason behind this robustness is not explained by an equilibrium of the core of the filament itself but by the fact that much larger propagation distances in turbulent air would be needed to strongly modify the 1 mm large energy reservoir and overcome the effect of the energy flux toward the filament axis.

IV. PROCEDURE FOR NUMERICAL SIMULATIONS

In order to discuss the results, we have performed numerical simulations. The propagation of ultrashort laser pulses and filamentation are described by means of a nonlinear evolution equation for the envelope $\mathcal{E}$ of the laser pulse along the z axis. The derivation of the equations of the model was reviewed in detail [Eqs. (47)–(51) in Ref. [1]]. We included a specific module in our simulation code for the description of the change of refraction index δn due to air turbulence. The propagation equation for the envelope of the laser pulse reads as

$$2ik_0\frac{\partial \mathcal{E}}{\partial z} + \Delta_\perp \mathcal{E} - 2ik_0 N(\mathcal{E}) = 2k_0^2 \delta n \mathcal{E}, \tag{6}$$

where $k_0=k(\omega_0)$ denotes the wave number corresponding to the central frequency ω_0. The term $\Delta_\perp$ in Eq. (6) represents the transverse Laplacian and accounts for beam diffraction; the third term $N(\mathcal{E})$ in Eq. (6) represents nonlinear effects which usually include the optical Kerr effect, multiphoton absorption, plasma defocusing, plasma absorption, and optical shock terms. Here, we performed a statistical analysis of filamentation in turbulent air and therefore considered only a reduced set of these effects for the bulk of the results, namely the optical Kerr effect with coefficient n_2 and multiphoton absorption with cross section β_K; K denotes the number of photons involved in the process:

$$N(\mathcal{E}) = i\frac{\omega_0}{c}n_2|\mathcal{E}|^2\mathcal{E} - \frac{\beta_K}{2}|\mathcal{E}|^{2K-2}\mathcal{E}. \tag{7}$$

Filamentation in the absence of air turbulence exhibits intensities usually saturated at levels which do not exceed a few 10^{13} W/cm^2 due to multiphoton absorption and defocusing due to the plasma generated by multiphoton ionization [28]. The multiphoton absorption cross section corresponds to the multiphoton ionization of oxygen atoms in air, for which $K=8$ photons are necessary at 800 nm to liberate an electron from an atom with ionization potential of 12.1 eV.

The right-hand side of Eq. (6) includes a source term that accounts for the effect of air turbulence on the refractive index fluctuations in air, described by a stochastic model of phase screens located along the propagation distance [29]. The power spectral density of the refractive index fluctuations is given by the modified von Karman spectrum

$$\psi_n(\kappa) = 0.033C_n^2(\kappa^2+\kappa_0^2)^{-11/6}\exp(-\kappa^2/\kappa_m^2), \tag{8}$$

where C_n^2 denotes the structure constant of atmospheric turbulence characterizing the magnitude of fluctuations, $\kappa_0=2\pi/L_0$ and $\kappa_m=5.92/l_0$, where $L_0=15$ cm and $l_0=1$ mm, denote the outer and inner scales of turbulence. These scales bound the inertial interval of turbulence where energy of the turbulent fluctuations is transferred from large to small eddies and eventually dissipated by viscosity. Each of the source terms was benchmarked independently by comparison with known analytical cases, or numerical solutions. For instance, the model was checked to correctly reproduce the average displacement of the center of mass of a low power beam in turbulent air [29].

The incoming pulse is assumed to be Gaussian in time and super-Gaussian of order $n=20$ in space so as to mimic the effect of a circular aperture used in the experiment; its envelope is described by

$$\mathcal{E}(x,y,t,z=0) = \mathcal{E}_0\exp[-(x^2+y^2)^{n/2}/w_0^n - t^2/t_p^2], \tag{9}$$

where $w_0=15$ mm is the beam width, $t_p=42$ fs is the pulse duration. The input intensity $\mathcal{E}_0^2 \equiv 2^{2/n}nP/2\pi w_0^2\Gamma(2/n)$ is computed from the input power $P=E_{in}/t_p\sqrt{\pi/2}$, which is computed from the pulse energy E_{in}. For $P=18P_{cr}$, the collapse distance of the super-Gaussian beam of order $n=20$ is obtained on-axis at $z=119$ m, after formation of a multiple ring profile which does not undergo collapse on itself [33]. The lens is modeled in both experiments by a spatial beam curvature $\exp[-ik_0(x^2+y^2)/2f]$. With the $f=4$ m lens, collapse of the super-Gaussian beam is obtained at 3.90 m without ring formation.

V. NUMERICAL RESULTS

We performed numerical simulations of the filamentation process in the experimental conditions for both cases A and B. In both cases and for all sets of simulations performed with similar turbulence (C_n^2, l_0, L_0) but different realizations of phase screens, we applied the statistical analysis presented in Sec. III. We show here typical results by using the same order in the presentation.

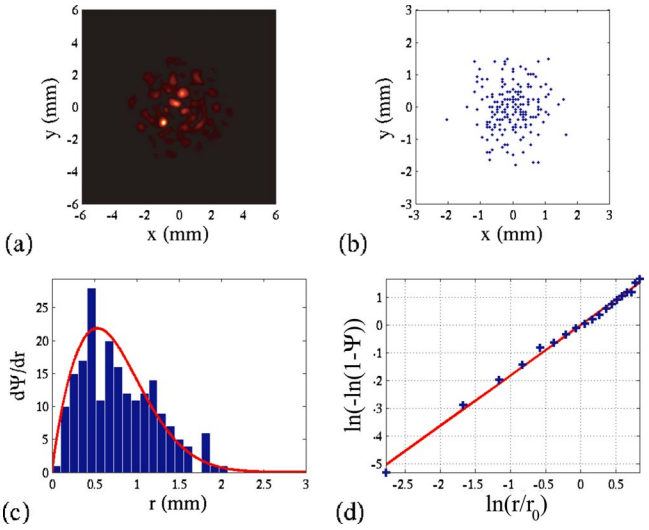

FIG. 8. (Color online) Numerical simulation results presented as in Fig. 4 for 200 shots in case A with strong turbulence $C_n^2=1.7\times10^{-11}$ m$^{-2/3}$. The probability function for the Weibull distribution [continuous curve in (c) and (d)] has parameters $p=1.81$ and $w_W=0.83$ mm.

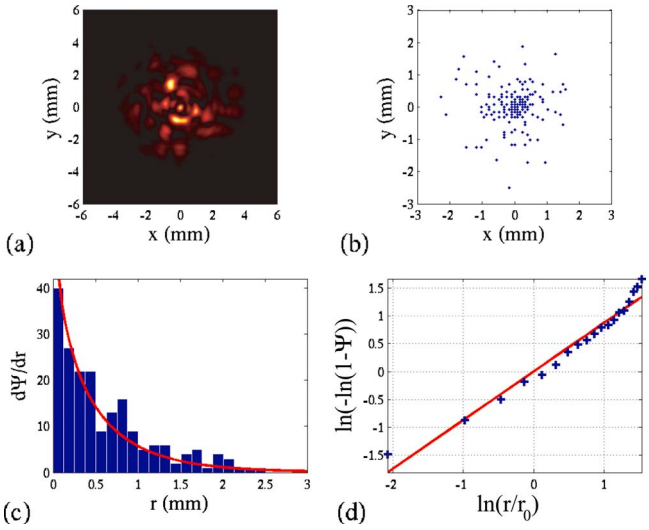

FIG. 10. (Color online) Numerical simulation results presented as in Fig. 4 for 200 shots in case A with the screen at $z=6$ m, weak turbulence $C_n^2=2.2\times10^{-12}$ m$^{-2/3}$. The parameters for the Weibull distribution [continuous curve in (c) and (d)] are $p=1.75$ and $w_W=0.73$ mm.

A. Simulations of case A

Simulation results when the pulse propagates through the turbulence cell before filamentation (case A) are shown in Figs. 8 and 9 for decreasing intensities of atmospheric fluctuations. Simulations were performed from the case of very strong turbulence ($C_n^2=9\times10^{-10}$ m$^{-2/3}$) to that of very weak turbulence ($C_n^2=2.1\times10^{-13}$ m$^{-2/3}$). Each set of simulations represents 200 shots. For very strong ($C_n^2=9\times10^{-10}$ m$^{-2/3}$) or strong (Fig. 8, $C_n^2=1.7\times10^{-11}$ m$^{-2/3}$) turbulence, the distribution of filaments can be correctly described by a Weibull distribution with parameters p slightly smaller than 2, indicating that the pointing instability after the filamentation stage follows the laws expected from homogeneous and isotropic turbulence acting on the whole path. The parameter w_W can be interpreted as a measure of the pointing instability and is observed to decrease when the turbulence strength decreases.

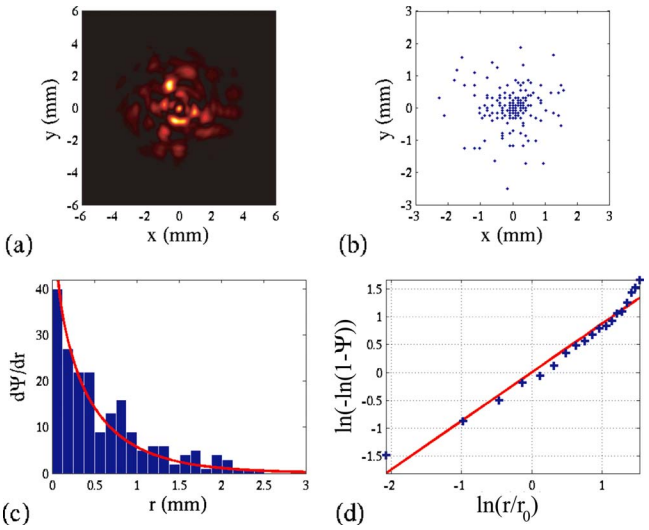

FIG. 9. (Color online) Numerical simulation results presented as in Fig. 4 for 200 shots in case A with the screen at $z=7$ m, weak turbulence $C_n^2=2.2\times10^{-12}$ m$^{-2/3}$. The Weibull distribution [continuous curve in (c) and (d)] has parameters $p=0.87$ and $w_W=0.50$ mm.

For weak (Fig. 9, $C_n^2=2.2\times10^{-12}$ m$^{-2/3}$) or very weak ($C_n^2=2.1\times10^{-13}$ m$^{-2/3}$) turbulence, the distribution of filaments can no longer be described by a Rayleigh-like distribution (i.e., a Weibull distribution with parameter p close to 2). The parameter of the Weibull distribution is indeed smaller than one in both cases, indicating that the probability to find a filament at distance r from the propagation axis is the largest on the axis ($r=0$). A similar distribution is observed experimentally for $C_n^2=2\times10^{13}$ m$^{-2/3}$ (see Fig. 5). This means that after the turbulence cell, the effects of linear focusing by the lens and of self-focusing of the whole beam due to the optical Kerr effect prevail over the effect of weak turbulence in the first propagation stage. This results in a minimal pointing instability which is still decreased as the intensity of turbulence decreases.

B. Competition between turbulence and ring formation

The results above highlight a competition between the effects of weak turbulence and both the linear and nonlinear effects playing a role in filamentation in the absence of turbulence, namely, diffraction and the optical Kerr effect. A striking feature of this competition is visible in Fig. 10 obtained from simulations of experiment A with weak air turbulence (similar results are obtained for very weak turbulence, data not shown). Figure 10(c) shows that the fit with the Weibull distribution function crudely fits the results. The reason for this poor agreement comes from the fact that there are intervals of the histogram in which we obtain an accu-

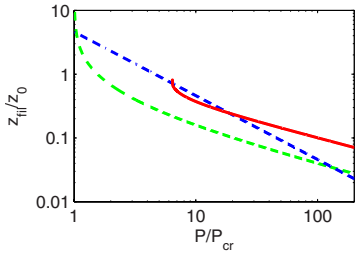

FIG. 11. (Color online) Filamentation distance as a function of P/P_{cr}: distance to observe a gain of 10^4 by MI (dash-dotted curve); collapse distance in nonturbulent air (dashed curve); and collapse distance in turbulent air (solid curve, $C_n^2=10^{-13}$ m$^{-2/3}$).

mulation of filaments. This is also clearly visible on the distribution of filaments [Fig. 10(b)] which exhibits rings where the filaments are preferentially located. These rings are formed because the input beam profiles are super-Gaussians so as to model the effect of the circular aperture. It is known that self-focusing of super-Gaussian beams forms rings [30] and that filaments in nonturbulent air locate preferentially on the largest intensity gradients of the beam [31,32]. A self-similar ringlike solution of the nonlinear Schrödinger equation was shown to exist and to behave as an attractor for the collapse dynamics of super-Gaussian beams [33]. Although the determination of the minimum power above which a ring collapse occurs is still an open question, it was shown that a radially symmetric ring collapse is obtained for input powers above $15P_{cr}$; in the presence of symmetry breaking inhomogeneities in the input beam, multiple filaments are formed as corroborated by experiments [34]. A competition therefore also exists between turbulence and the latter effect. Because of our relatively low powers, we observe a ring formation without any catastrophic ring collapse. For perfect radial symmetry, the filament would finally form on axis after refocusing of the whole beam, even if rings appear. In the presence of weak turbulence, modulational instability is enhanced and filaments form on the intense rings generated during the focusing stage. As shown below, this competition also explains the longitudinal wandering of filaments.

C. Interpretation of the longitudinal wandering of filaments in turbulent air

The competition between self-focusing of the whole beam and modulational instability (MI) was studied by Fibich *et al.* [35] who showed that for input powers smaller than $100P_{cr}$, self-focusing of the whole beam prevails and the collapse distance scales as $1/\sqrt{P}$, whereas for $P>100P_{cr}$, MI prevails and the collapse distance scales as $1/P$. This follows from the amplification rates k_i of small perturbations growing as $\exp(k_i z)$, given by $k_i z_0=k_\perp w_0\sqrt{P/P_{cr}-k_\perp^2 w_0^2/16}$, the propagation distance where z_0, the Rayleigh length associated with the beam of diameter w_0, makes the growth rates dimensionless. The maximum growth rate is $k_i^{max}z_0=2P/P_{cr}$ and yields an amplification by a factor of, e.g., 10^4 over a distance $z=z_0\times 2\log(10)P_{cr}/P$.

Figure 11 shows as a dashed curve the distance z_{fil} at which a filament would form in a nonturbulent atmosphere, as given by Marburger's law for the collapse of optical beams in Kerr media and scaling roughly as $(P/P_{cr})^{-1/2}$ [36]. The dash-dotted line shows the distance required for MI to amplify narrow perturbations by a factor of 10^4; this distance is smaller than the collapse distance z_{fil} for powers above $200P_{cr}$, which means that self-focusing of the whole beam is the prevailing mechanism in the formation of filaments at smaller powers.

In a turbulent atmosphere, the distance required for self-focusing of the whole beam was shown by Petrishchev [24] to be determined by the zeros of the function

$$1+(1-P/P_{cr})(z/z_0)^2+\frac{k^3w_0^4C}{8}(z/z_0)^3=0, \qquad (10)$$

where C is given by Eq. (2). A filament formed in a turbulent atmosphere begins at this collapse distance which is plotted as a function of P/P_{cr} in Fig. 11(b) (solid curve) for $C_n^2=10^{-13}$ m$^{-2/3}$ and the conditions of our experiments. Filaments obtained by self-focusing of the whole beam thus start at larger distances when turbulence is increased. As a result, the power threshold above which MI starts to be the prevailing mechanism to form a filament is smaller than that predicted by using Marburger's collapse distance. Figure 11(b) shows that the solid curve ($C_n^2=10^{-13}$ m$^{-2/3}$) intersects the dash-dotted line (MI) around $20P_{cr}$, which gives a reduction by a factor of 10 for the power threshold to form filaments by MI, in the condition of our experiments. Since the distance required for MI and amplification of turbulence induced noise decreases when turbulence is increased, our conditions belong to the region where self-focusing of the whole beam competes with MI to form filaments. These results also explain the average decrease of the collapse and filamentation distance obtained by Kandidov *et al.* [10] when turbulence is increased. In this respect, we computed the minimal distance for which the peak intensity exceeds a certain threshold, for each of the 200 shots corresponding to each value of the structure constant C_n^2 in case A. Results are shown in Figs. 12 and 13. For strong turbulence, filamentation starts on the average before the nonlinear focus at 390 cm obtained for the same input conditions but without turbulence. For weak turbulence, the average beginning of filamentation is shifted beyond the focus of the lens. This result does not depend on the choice of the intensity threshold to perform these statistics as shown by a comparison of Figs. 12 and 13. However, the filamentation rate defined here as the number of shots for which the peak intensity exceeds the chosen threshold is strongly dependent on the threshold. This is explained by the fact that due to saturation, the peak intensity for a filament in nonturbulent air reaches a few 10^{13} W/cm^2 [28]; the saturation value decreases when the strength of turbulence increases, thus the filamentation rate decreases when C_n^2 increases or when the intensity threshold is chosen larger.

We finally note that our use of the simplest form of MI theories, which applies for perturbations of plane waves, leads to a larger value ($200P_{cr}$ for the threshold above which MI prevails) than the value that would be obtained by considering MI of a Townes profile [37] or MI of a ring solution

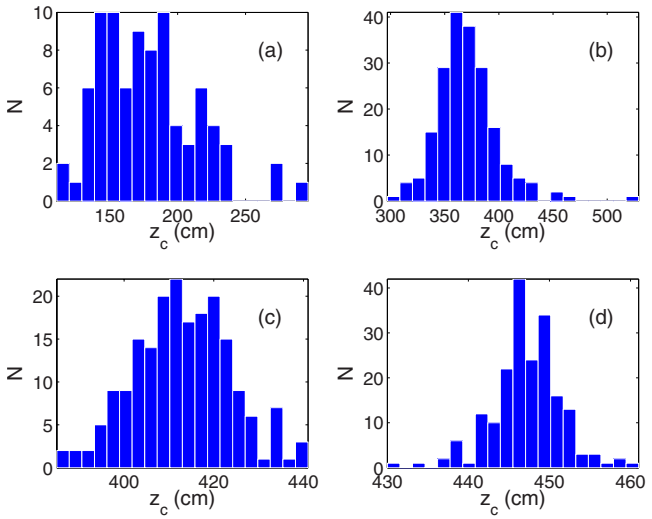

FIG. 12. (Color online) Distribution of filamentation distances, defined as the minimal distance for which the peak intensity exceeds the threshold of 10^{13} W/cm^2 in case A. The focus of the lens is at 400 cm and the collapse distance without turbulence is at 390 cm. The statistics is performed over 200 shots for each C_n^2. (a) $C_n^2=9\times10^{-10}$ m$^{-2/3}$. (b) $C_n^2=1.7\times10^{-11}$ m$^{-2/3}$. (c) $C_n^2=2.2\times10^{-12}$ m$^{-2/3}$. (d) $C_n^2=2.1\times10^{-13}$ m$^{-2/3}$. The peak intensity is below threshold for 57% of the shots in case (a), 1% in case (b), and is above threshold in cases (c) and (d).

[34]. The principle of our analysis would, however, be the same with a different type of beam profile, for which qualitative agreement with our results is expected.

D. Simulations in case B

Figure 14 shows the statistical analysis of simulation results in case B for very strong turbulence. Figure 14(a) clearly shows that the energy reservoir exhibits rings which are the result of several effects, among which diffraction of the apertured input beam, self-focusing of this super-Gaussian-like beam, as well as the competition between diffraction and multiphoton absorption, which acts as a distributed stopper along the filament, thus generating diffraction rings [38]. Turbulence plays a role only after the energy reservoir has been reshaped into rings. Therefore the action of turbulence on the intense core is limited to a moderate tilt of the filament. The larger scale energy flux toward the propagation axis is in principle more sensitive to air turbulence but multiphoton absorption in the filament core prevails in sustaining the energy flux and its symmetry. This leads to an overall weak effect of turbulence on already formed filaments, in agreement with experimental results.

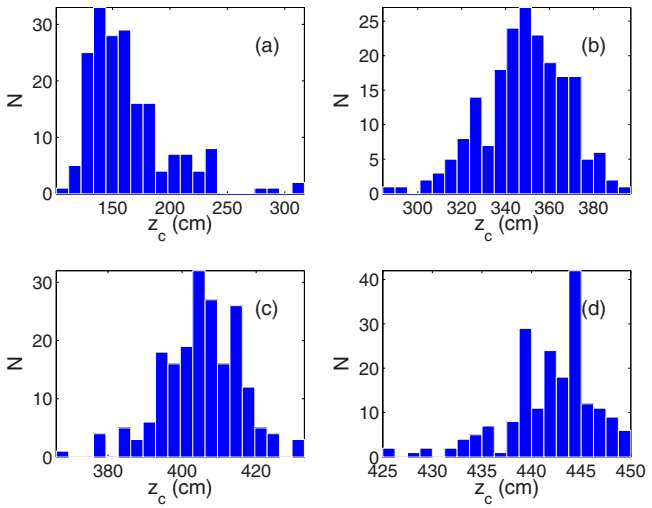

FIG. 13. (Color online) Same as in Fig. 12 but for the threshold of 8×10^{12} W/cm^2. The peak intensity remains below threshold for 7% of the shots for (a) $C_n^2=9\times10^{-10}$ m$^{-2/3}$ and is above threshold for all shots for weaker turbulence (b)–(d).

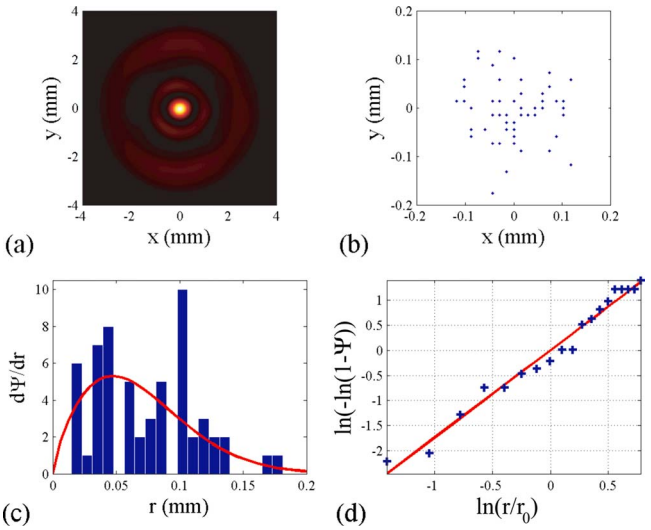

FIG. 14. (Color online) Numerical simulation results presented as in Fig. 4 for 60 shots in case B with the screen at $z=6$ m, very strong turbulence $C_n^2=9\times10^{-10}$ m$^{-2/3}$. The parameters for the Weibull distribution [continuous curve in (c) and (d)] are $p=1.74$ and $w_W=0.077$ mm.

VI. CONCLUSIONS

The influence of air turbulence on the filamentation of ultrashort laser pulses close to one critical power is studied experimentally with a calibrated turbulence chamber reproducing over 2.3 m various atmospherical conditions. The transverse deviation of the filament and its survival rate in the presence of turbulence are accurately measured for different scenarios where the filaments form either in quiet or in turbulent atmosphere. For each case the statistical filament transverse deviation is well-fitted by a Weibull distribution law and the average deviation increases with turbulence. These measurements are well-reproduced by numerical simulations.

Turbulence strongly affects the transverse wandering of filaments even if the average deviation is smaller when the filament is formed in nonturbulent air. When the laser beam undergoes strong turbulence during the initial self-focusing stage as in outdoor experiments, the filamentation rate decreases and a larger filament pointing instability is observed. The decrease of the probability to form a filament in this case

tends to prove that the collapse distance increases in the presence of turbulence. On the contrary, femtosecond filaments generated in air are robust and barely sensitive to turbulence if they are formed in a nonturbulent region. We interpreted the longitudinal wandering of filaments in two different regimes where either modulational instability or self-focusing of the whole beam constitutes the prevailing effect in forming a filament. Self-focusing of the whole beam leads to different scenarios for small powers, strong trubulence, which promotes homogeneous and isotropic filament distributions or for larger powers, weak turbulence, which promotes ring formation and accumulation of filaments on collapsing rings.

ACKNOWLEDGMENT

This work has been partially funded by a DGA grant.

[1] A. Couairon and A. Mysyrowicz, Phys. Rep. **441**, 47 (2007).
[2] G. Méchain, C. D'Amico, Y.-B. André, S. Tzortzakis, M. Franco, B. Prade, A. Mysyrowicz, A. Couairon, E. Salmon, and R. Sauerbrey, Opt. Commun. **247**, 171 (2005).
[3] J. Kasparian, M. Rodriguez, G. Méjean, J. Yu, E. Salmon, H. Wille, R. Bourayou, S. Frey, Y.-B. André, A. Mysyrowicz, R. Sauerbrey, J.-P. Wolf, and L. Wöste, Science **301**, 61 (2003).
[4] A. Houard, C. D'Amico, Y. Liu, Y. B. André, M. Franco, B. Prade, E. Salmon, P. Pierlot, L.-M. Cléon, and A. Mysyrowicz, Appl. Phys. Lett. **90**, 171501 (2007).
[5] C. D'Amico, A. Houard, M. Franco, B. Prade, A. Mysyrowicz, A. Couairon, and V. T. Tikhonchuk, Phys. Rev. Lett. **98**, 235002 (2007).
[6] C. D'Amico, A. Houard, S. Akturk, Y. Liu, J. Le Bloas, M. Franco, B. Prade, A. Couairon, V. T. Tikhonchuk, and A. Mysyrowicz, New J. Phys. **10**, 013015 (2008).
[7] V. E. Zuev, *Laser Beams in the Atmosphere* (Consultants Bureau, New York, 1982).
[8] V. I. Tatarskii, *Wave Propagation in Turbulent Medium* (McGraw-Hill, New York, 1961); *The Effects of the Turbulent Atmosphere on Wave Propagation* (U.S. Departement of Commerce, National Technical Information Service, Springfield, VA, 1971).
[9] J. R. Penano, P. Sprangle, B. Hazafi, A. Ting, D. F. Gordon, and C. A. Kapetanakos, Phys. Plasmas **11**, 2865 (2004).
[10] V. P. Kandidov, O. G. Kosareva, M. P. Tamarov, A. Brodeur, and S. L. Chin, Quantum Electron. **QE-29**, 911 (1999).
[11] V. I. Bespalov and V. I. Talanov, Zh. Eksp. Teor. Fiz. Pis'ma Red. **3**, 471 (1966) [JETP Lett. **3**, 307 (1966)].
[12] A. Couairon, Appl. Phys. B: Lasers Opt. **76**, 789 (2003).
[13] S. Tzortzakis, G. Méchain, G. Patalano, M. A. Franco, B. S. Prade, and A. Mysyrowicz, Appl. Phys. B: Lasers Opt. **76**, 609 (2003).
[14] A. Couairon, G. Méchain, S. Tzortzakis, M. Franco, B. Lamouroux, B. Prade, and A. Mysyrowicz, Opt. Commun. **225**, 177 (2003).
[15] S. L. Chin, A. Talebpour, J. Yang, S. Petit, V. P. Kandidov, O. G. Kosareva, and M. P. Tamarov, Appl. Phys. B: Lasers Opt. **74**, 67 (2002).
[16] R. Ackermann, G. Méjean, J. Kasparian, J. Yu, E. Salmon, and J.-P. Wolf, Opt. Lett. **31**, 86 (2006).
[17] R. Salamé, N. Lascoux, E. Salmon, R. Ackermann, J. Kasparian, and J.-P. Wolf, Appl. Phys. Lett. **91**, 171106 (2007).
[18] M. Mlejnek, M. Kolesik, J. V. Moloney, and E. M. Wright, Phys. Rev. Lett. **83**, 2938 (1999).
[19] M. Kolesik and J. V. Moloney, Opt. Lett. **29**, 590 (2004).
[20] W. Liu, J.-F. Gravel, F. Théberge, A. Becker, and S. L. Chin, Appl. Phys. B: Lasers Opt. **80**, 857 (2005).
[21] A. Dubietis, E. Gaižauskas, G. Tamošauskas, and P. Di Trapani, Phys. Rev. Lett. **92**, 253903 (2004).
[22] D. Faccio, A. Averchi, A. Lotti, P. Di Trapani, A. Couairon, D. Papazoglou, and S. Tzortzakis, Opt. Express **16**, 1565 (2008).
[23] P. Polesana, M. Franco, A. Couairon, D. Faccio, and P. Di Trapani, Phys. Rev. A **77**, 043814 (2008).
[24] V. A. Petrishchev, Izv. Vyssh. Uchebn. Zaved., Radiofiz. **14**, 1416 (1971).
[25] M. Billard, G. Fertin, and J. C. Fontanella, *Atmospheric Turbulence Simulation Cell for Optical Propagation Experiment*, 4th International Symposium on Gas Flow and Chemical Lasers, Stresa (Italy), 1982 (unpublished).
[26] S. S. R. Murty and W. Bilbro, Atmospheric Effects on CO_2, Laser Propagation, NASA Technical Paper 1357, 1978 (unpublished).
[27] R. R. Beland, in *IR/EO Systems Handbook*, edited by F. G. Smith (SPIE Optical Engineering Press, Ann Arbor, 1993), Vol. 2, pp 157–232.
[28] A. Couairon, Phys. Rev. A **68**, 015801 (2003).
[29] J. M. Martin and S. M. Flatte, Appl. Opt. **27**, 2111 (1988).
[30] A. Couairon, S. Tzortzakis, L. Bergé, M. Franco, B. Prade, and A. Mysyrowicz, J. Opt. Soc. Am. B **19**, 1117 (2002).
[31] G. Méchain, A. Couairon, M. Franco, B. Prade, and A. Mysyrowicz, Phys. Rev. Lett. **93**, 035003 (2004).
[32] G. Méchain, A. Couairon, Y.-B. André, C. D'Amico, M. Franco, B. Prade, S. Tzortzakis, A. Mysyrowicz, and R. Sauerbrey, Appl. Phys. B: Lasers Opt. **79**, 379 (2004).
[33] G. Fibich, N. Gavish, and X.-P. Wang, Physica D **211**, 193 (2005).
[34] T. D. Grow, A. A. Ishaaya, L. T. Vuong, A. L. Gaeta, N. Gavish, and G. Fibich, Opt. Express **14**, 5468 (2006).
[35] G. Fibich, S. Eisenmann, B. Ilan, Y. Erlich, M. Fraenkel, Z. Henis, A. L. Gaeta, and A. Zigler, Opt. Express **13**, 5897 (2005).
[36] J. H. Marburger, Prog. Quantum Electron. **4**, 35–110 (1975).
[37] M. A. Porras, A. Parola, D. Faccio, A. Couairon, and P. Di Trapani, Phys. Rev. A **76**, 011803(R) (2007).
[38] D. Faccio, M. Clerici, A. Averchi, O. Jedrkiewicz, S. Tzortzakis, D. G. Papazoglou, F. Bragheri, L. Tartara, A. Trita, S. Henin, I. Critiani, A. Couairon, and P. Di Trapani, Opt. Express **16**, 8213 (2008).